

Debonding failure analysis of prestressed FRP strengthened RC beams

Nusrat Hoque^{1a} and Mohd Z. Jumaat^{*2}

¹Department of Civil Engineering, University Malaya, Jalan University, 50603, Kuala Lumpur, Malaysia

²Department of Civil Engineering, University Malaya, 50603, Kuala Lumpur, Malaysia

(Received September 17, 2016, Revised November 26, 2017, Accepted March 9, 2018)

Abstract. Fiber Reinforced Polymer (FRP), which has a high strength to weight ratio, are now regularly used for strengthening of deficient reinforced concrete (RC) structures. While various researches have been conducted on FRP strengthening, an area that still requires attention is predicting the debonding failure load of prestressed FRP strengthened RC beams. Application of prestressing increases the capacity and reduces the premature failure of the beams largely, though not entirely. Few analytical methods are available to predict the failure loads under flexure failure. With this paucity, this research proposes a method for predicting debonding failure induced by intermediate crack (IC) for prestressed FRP-strengthened beams. The method consists of a numerical study on beams retrofitted with prestressed FRP in the tension side of the beam. The method applies modified Branson moment-curvature analysis together with the global energy balance approach in combination with fracture mechanics criteria to predict failure load for complicated IC-induced failure. The numerically simulated results were compared with published experimental data and the average of theoretical to experimental debonding failure load is found to be 0.93 with a standard deviation of 0.09.

Keywords: debonding; fracture energy; FRP strengthening; global energy balance; prestressing

1. Introduction

RC structures are strengthened for many reasons, such as an increase in load requirement, degradation due to structural aging, and faulty design or construction. Strengthening of structures is a more viable, cost effective, and time effective solution than demolishing and replacing the entire structures (Ghasemi *et al.* 2015, Matthys 2000, Raafat and Mohamed 2011). Advanced composites, such as FRP, are preferred materials for strengthening due to their high tensile strength, lightweight nature, corrosion resistance capacity, high durability, and ease of installation. Strengthening of RC beams using carbon FRP, in particular, has received much attention from researchers. However, flexural tests of strengthened beams show a brittle type of premature failure, by the debonding of FRP laminate from the concrete, where the tensile capacity of FRP laminates was well below the ultimate capacity of the FRP laminate. For this, in spite of huge potential, FRP laminate could not be utilized efficiently in strengthening due to this premature failure (Oehlers *et al.* 2000a, 2000b). To address the serviceability issue of FRP strengthened members prestressing has been used in FRP strengthening purpose (Oudah and El-Hacha 2011). Since 1990's, some researchers' employed this technique by prestressing the FRP laminate prior to attaching the beam which obviously could utilize the tensile capacity of the FRP more efficiently

than the unstressed FRP (El-Hacha *et al.* 2001, Nordin and Täljsten 2006, Pellegrino and Modena 2009, You *et al.* 2012, Yu *et al.* 2008).

In addition to the utilization of the utmost capacity of the FRP, prestressing the tension reinforcement of RC beam also reduce the crack formation and increase its capacity. Therefore, the failure analysis of prestressed beam is one of the significant research fields in strengthening. Despite of significant progress in the experimental work of prestressed strengthened beam using the different prestressing technique, prestressing percentage etc., there has been a very little study made on predicting the debonding failure of this type of beam analytically or numerically. FRP rupture is the prominent failure mode for strengthened prestressed beam. However, intermediate crack induced (IC) debonding type failure, is mainly observed for prematurely failed beams. This type of failure typically initiated from the location of major flexure or flexure-shear crack near the load application point and travels towards the end of the beam. On the other hand, concrete cover separation type failure initiating from the FRP curtailment location and propagating towards the center of the beam, commonly known as plate end (PE) debonding (Rezazadeh *et al.* 2016) is rarely observed.

There are few analytical studies available for predicting the ultimate failure of the prestressed beams like concrete crushing and steel yielding. Barros *et al.* (2012) developed a design-oriented model to determine the moment-curvature response of a rectangular cross section of FRC (Fiber reinforced concrete) members prestressed by longitudinal prestressed steel and FRP bars failed in flexure. Kara *et al.* (2016) also developed a numerical method for estimating the response of beam strengthened with NSM FRP bars and

*Corresponding author, Professor

E-mail: zamin@um.edu.my

^aPh.D. Student

E-mail: nusrat_hoque@yahoo.com

strips using sectional analysis. Hajihashemi *et al.* (2011) also estimate the response using sectional analysis. Rezazadeh *et al.* (2014), Xue *et al.* (2010) and Woo *et al.* (2008) simulate the prestressed strengthened beam response using nonlinear finite element approach. Rezazadeh *et al.* (2015) proposed an analytical method to simulate the flexural behaviour of prestressed CFRP strengthened RC beams. The proposed model was checked for RC beams strengthened using prestressed NSM FRP failed by conventional flexural mode and good accuracy was found. Moreover, the model was used to check the efficiency against concrete cover failure for non-prestressed FRP strengthened beam. However, very few works are available for estimating the premature failure of strengthened beam with prestressed FRP. With this aim, this paper focuses on developing a numerical model for predicting the IC debonding of prestressed FRP strengthened beam.

Several models are available for predicting IC debonding of non-prestressed strengthened beam. Some available models of IC debonding are provided by Wang and Li (1998), Sebastian (2001), Teng *et al.* (2002), Teng *et al.* (2003), Teng *et al.* (2004), Malek *et al.* (1998), Rahimi and Hutchinson (2001), Lu *et al.* (2007) based on either mechanics or fracture theories or finite element (FE) analysis. However, strength based model can predict the local failure but not the global failure of the beam.

Some researchers (Niu and Wu 2001) uses the fracture energy as the failure criteria for determining the IC debonding failure by limiting the force transferred by the FRP in strengthened beam by comparing it with the maximum pull force endured by FRP obtained from the simple shear test. Dai *et al.* (2008) proposed a failure criterion for IC debonding using the bond-properties of FRP-concrete interface and the geometric and material properties of the beam. On the other hand, several codes, such as ACI-4402R-08 (2008) and TR-55 (2012) adopt some guidelines for IC debonding which is solely based on the simple shear test specimen. Although several similarities are observed between IC debonding and failure behavior in a simple shear test, subtle difference is also found. Rosenboom and Rizkalla (2008) evaluated some of these models and showed poor correlation with the experimental data of IC debonding failure. They proposed an analytical model based on the interface shear stress using the concrete shear strength as the failure criteria.

Meanwhile, Hearing and Buyukozturk (2000), Gunes *et al.* (2009), and Achintha and Burgoyne (2008) focused on energy-based solutions using fracture mechanics criteria to predict debonding failure of the FRP strengthened beams. The models by Hearing and Buyukozturk (2000) and Gunes *et al.* (2009) can only predict PE debonding, whereas the model by the latter group of authors can predict PE and IC debonding. The latter model also eliminates the major disadvantages of the two previous models, such as the assumption of constant curvature and linear elasticity.

The current study proposes a model for simulating the behavior of prestressed FRP-strengthened RC beams by applying the model proposed by Achintha and Burgoyne (2008) for prestressed FRP strengthened beam. A moment-curvature model for prestressed FRP strengthened RC beams is established first using modified Branson method

and then the debonding model proposed by Achintha and Burgoyne (2008) is applied to predict debonding failures. The proposed prediction model is validated against published experimental models.

2. Numerical approach

The debonding analysis of prestressed beam with GEBA requires computation of the strain energy in the beam. The strain energy in a beam at any loading state can be found from the energy that is recoverable upon complete unloading. This recoverable energy can also be determined from the computation of work done on the beam as proposed by Achintha and Burgoyne (2009). For beams used in practical purpose, significant energy contribution can be caused due to bending deformation. Thus, the work done on any beam can be approximated as the summation of bending deformation as in Eq. (1)

$$W_{beam} = \int V M \kappa dV, \quad (1)$$

where W_{beam} is the work done on the beam; And $M-\kappa$ are the moment and curvature respectively.

Thus, the first step is to determine the $M-\kappa$ relationship of any beam for energy evaluation. In this paper, a numerical method will be described for estimating the curvature, deflection and moment carrying capacity of beams strengthened with prestressed externally bonded reinforced (EBR) as well as Near surface mounted (NSM) reinforcement. The method is the extension of moment-curvature analysis of beam for non-prestressed EBR-FRP strengthened beam proposed by (Achintha and Burgoyne 2009). The uniqueness of the method is the decoupling of the FRP plate with the assumption that FRP will not act as a second layer of reinforcement rather it will act as a prestressing force to the beam inducing force and moment to it. This decoupling is necessary in order to apply the Branson's (1968) formula for determining the stiffness of partially cracked section to include the effect of tension stiffening because the applicability of Branson method is limited to RC section only.

2.1 Mechanical behaviour of constituent materials

The constitutive material properties used for simulating the $M-\kappa$ relationship of prestressed FRP strengthened RC beams are summarized in this section. Parabolic stress-strain curve proposed by Hognestad (1951) is assumed for concrete in compression and for concrete, under tension, a linear elastic behaviour is assumed with the same modulus as the initial modulus in compression as shown in Fig. 1(a) and (b). The tensile strength in rupture f_t and modulus of elasticity E_c are determined using relationship provide by ACI-CODE (2008) as in Eqs. (2) and (3).

$$f_t = 0.62\sqrt{f_c'} \left(\frac{N}{mm^2} \right) \text{units} \quad (2)$$

$$E_c = 4733\sqrt{f_c'} \left(\frac{N}{mm^2} \right) \text{units} \quad (3)$$

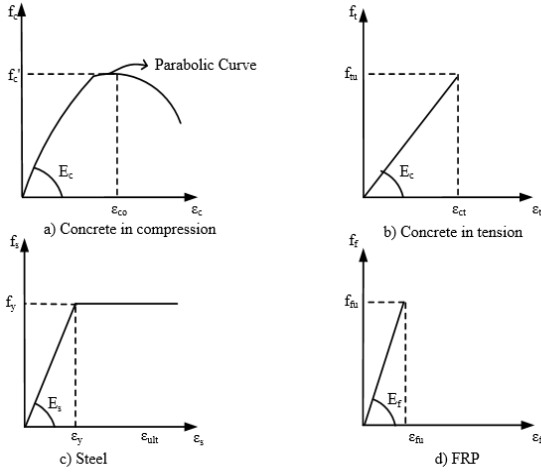


Fig. 1 Material properties

where f'_c is the compressive strength of concrete.

Steel and FRP properties adopted in the simulation are shown in Fig. 1(c) and (d). The steel is modeled with general elastic-perfectly plastic material and FRP as elastic material till rupture point respectively.

2.2 Moment-curvature of prestressed beam

A strengthened beam can have three types of sections: uncracked, fully cracked, and partially cracked. In the uncracked type, the applied moment on the beam is less than the cracking moment, M_{cr} , of the section. Thus, the beam does not have any crack in it at this stage. In the fully cracked type, the applied moment on the section is greater than the yield moment capacity, M_y , of the beam. In other words, tension steel in the beam is yielded. In the partially cracked type, the section is neither uncracked (i.e., the concrete already starts to crack) nor fully cracked (i.e., steel is not yielded). Once the mechanical properties of materials are chosen, the strain at any uncracked or fully cracked section of the beam can be determined by solving the force equilibrium and moment equilibrium conditions given in Eqs. (4) and (5) (Rezazadeh *et al.* 2015). The iterative program is run using MATLAB for every 1 mm section of the beam to solve these equations and finding the strain at two extreme fibers. This strain can be used then to determine the depth of neutral axis (x) for the corresponding section and hence the curvature of the section (κ).

The contribution of axial force in the FRP has to be included in the analysis. Since this M- κ model separates the FRP force from the analysis, so the determination of FRP force is obtained by strain compatibility with the extreme tension fiber using trial error process.

$$\sum F = C_c + T'_s - C_t - T_s - T_{frp} = 0 \quad (4)$$

$$\sum M = C_c * (x - \gamma x) + T'_s(x - dc) + C_t(2 * (h - x)/3) + T_s(d - x) + T_{frp}(h_f - x) = M_{ext} \quad (5)$$

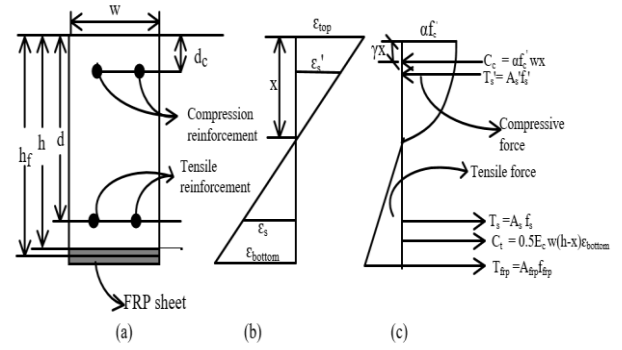


Fig. 2 Stress-strain distribution of prestressed beam

Where C_c is the compressive force due to concrete, x is the depth of neutral axis, γx is the depth of concrete compressive force from the top of the beam, T'_s is the compressive force due to top steel, d_c is the depth of compression steel from top fiber, C_t is the tensile force due to concrete below neutral axis, h is the height of the beam, T_s is the tension force due to tension steel, d is the depth of tension steel from top fiber, T_{frp} is the force in FRP, h_f is the depth of FRP from the top fiber, E_c is the elastic modulus of concrete and f_s , f'_s , and f_{frp} are the stress in the tension, compression, and FRP reinforcement respectively, where stress is the product of elastic modulus of the reinforcement and the strain at any stage. M_{ext} is the moment applied at any section for any load. All the symbols are defined graphically in Fig. 2. C_t is considered zero for the fully cracked section because the contribution of concrete at the fully cracked stage is zero. The strain at bottom fiber of a prestressed beam as shown in Fig. 2 would be

$$\varepsilon_{bottom} = \varepsilon_{frp} - \varepsilon_{pre} \quad (6)$$

So, the force in FRP will be as expressed in Eq. (7).

$$f_{frp} = \varepsilon_{frp} * E_{frp} = (\varepsilon_{bottom} + \varepsilon_{pre}) * E_{frp} \quad (7)$$

ε_{pre} is the prestressing strain applied to the FRP reinforcement for a corresponding force of P_{pre} , ε_{frp} is the total strain in the FRP and E_{frp} is the elastic modulus of FRP.

Since all the computation is done with the consideration of decoupling FRP force from the beam, so the RC section has to be analyzed for a combined action of a compressive force and moment acting the RC section alone. The moment acting on RC section alone can be separated from the moment resisted by the FRP force if only the centroid of the beam is known.

In the case of a non-linear, non-homogeneous section like RC, centroid, and neutral axis depth continuously changes. So mid-depth axis is chosen as the reference axis for decoupling the force as proposed by Achintha and Burgoyne (2008) instead of centroidal axis. Hence the moment that will be acting purely on the RC section can be computed using the expression in Eq. (8).

$$M_{A-y} = M_{applied} - T_{frp} \times (h_f - y) \quad (8)$$

Where 'A-y' refers to the moment acting on RC section alone about the axis y. In that case, A can be cracking (cr),

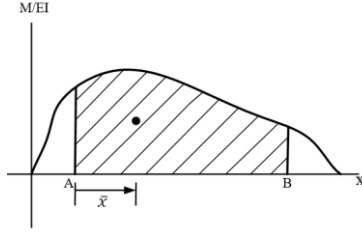


Fig. 3 Graphical representation of moment-area theorem

yield (y) or applied (app) moment and y could be mid-height of the beam (mid), i.e., $(h/2)$ or centroidal axis depth (α_{eff}).

The prestressing of FRP sheets in the strengthening of RC beams will increase the cracking as well as yield moment i.e., it will delay the yielding of steel and hence failure load will also increase than the non-prestressed strengthened beam. The increase in the first cracking moment and the yielding moment could be calculated using the following relationship

$$M_{inc_cr} = A_{frp} E_{frp} \epsilon_{pre} (h_f - x_{cr}) \quad (9)$$

$$M_{inc_yield} = A_{frp} E_{frp} \epsilon_{pre} (h_f - x_y) \quad (10)$$

x_{cr} and x_y are the depth of compression fiber of beam from the center of the beam for uncracked stage and yield stage.

So, the cracking moment M_{cr} and yield moment M_y for the prestressed beam will be

$$M_{cr} = \frac{f_t x_{cr}}{I_g} + M_{inc_cr} \quad (11)$$

$$M_y = f_a x_y^2 w (1 - \gamma) + A'_s E_s \epsilon'_s (x_y - d_c) + A_s f_y (d - x_y) + A_f E_{frp} \epsilon_{frp} + M_{inc_yield} \quad (12)$$

Where f_t tensile strength of concrete during rupture, I_g is the gross moment of inertia and other symbols are already defined earlier. The negative curvature of the beam at the uncracked stage will be

$$k_{pre} = \frac{\epsilon_{top_pre}}{x_{pre}} \quad (13)$$

Where ϵ_{top_pre} is the strain at the top fiber of the beam due to prestressing and x_{pre} is the corresponding depth for neutral axis. For partially cracked section the sectional strain, curvature, neutral axis depth can be determined by applying modified Branson (1968) concept as discussed by Achintha and Burgoyne (2009) adopted for FRP section. Originally Branson's model was conceived only for conventional RC beams with steel reinforcement up to steel yield level. So, considering added FRP with different bond characteristics as the second layer of reinforcement is thereby inappropriate. On the other hand, the model has to work beyond steel yield. So, Achintha and Burgoyne addressed these issues for applying Branson's model in FRP strengthened beam and proposed the following expressions for determining the effective stiffness of FRP strengthened beam.

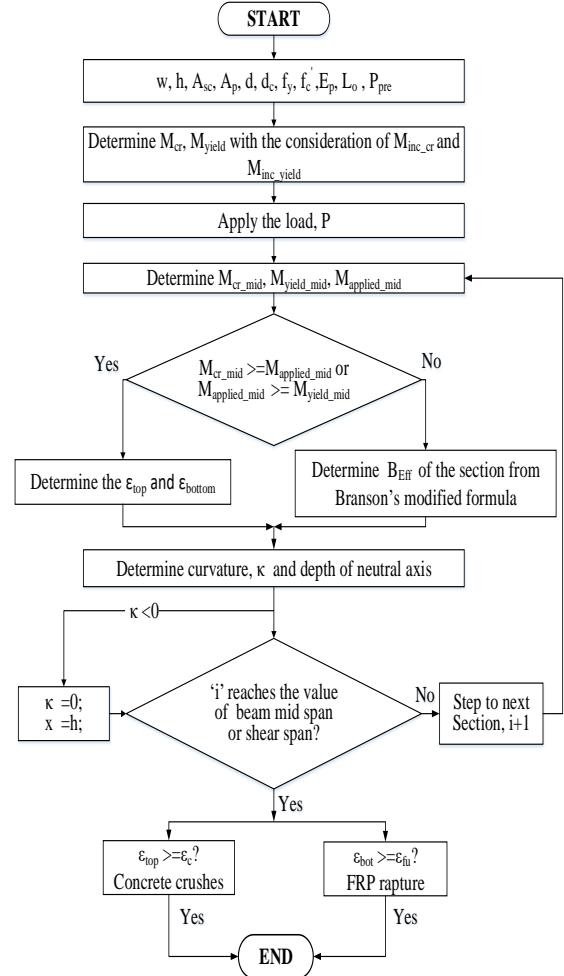


Fig. 4 Flow chart of moment-curvature for prestressed FRP strengthened beam

$$B_{eff} = K_p B_{uc} + (1 - K_p) B_{fc} \quad (14)$$

$$K_p = (M_{cr-mid} / M_{applied-mid})^4 \left[1 - \frac{M_{applied-mid} - M_{cr-mid}}{M_{yield-mid} - M_{applied-mid}} \right]^4 \quad (15)$$

Where B_{uc} and B_{fc} are stiffness of uncracked and yielded section respectively. M_{cr-mid} , $M_{applied-mid}$ and $M_{yield-mid}$ can be determined using Eq. (8). Once B_{eff} is determined for partially cracked section, the curvature of the section will be

$$\kappa = \frac{M_{eff}}{B_{eff}} \quad (16)$$

Where M_{eff} can be determined using Eq. (8) by putting α_{eff} as ' y '. Here α_{eff} is the depth of centroidal axis as will be discussed in the following section.

After determining strain and curvature, the deflection value at the midspan is determined using the classical second-moment area theorem in MATLAB (Hibbeler 2012). According to the second theorem the vertical deviation ' $t_{A/B}$ ' of any point 'A' on the elastic curve with respect to the tangent extended from another point 'B' is moment of the

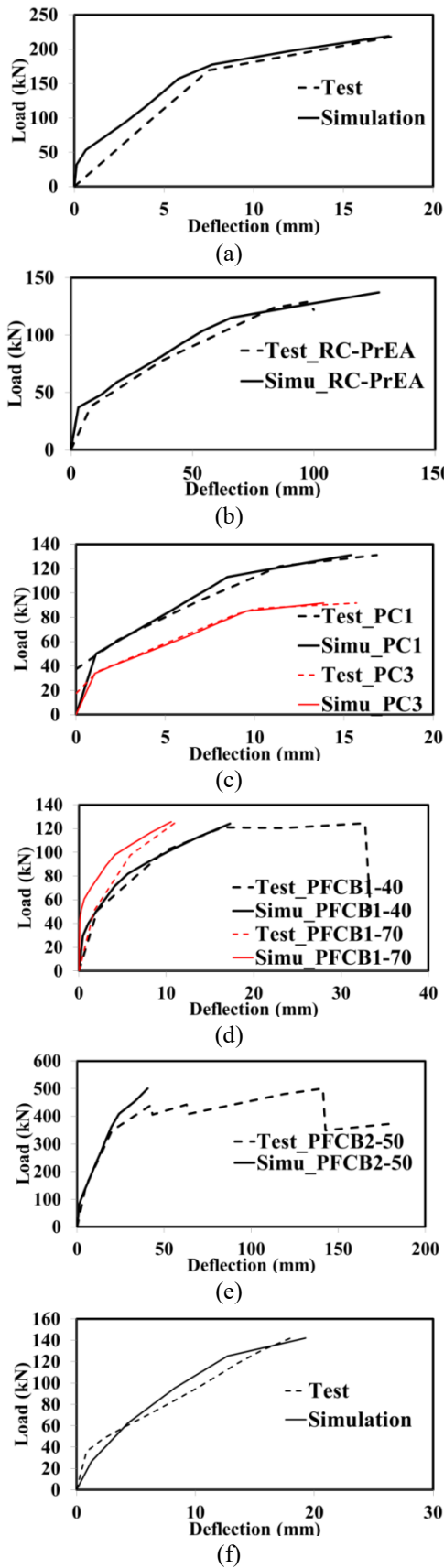


Fig. 5 Load-deflection curve for beam tested by (b) Pelligrino *et al.* (2009) (c) PC-1 and PC-3 by Xue *et al.* (2010) (d) PCFCB1-40 and PCFCB1-70 (e) PCFCB2-50 by You *et al.* (2012) (f) P4 tested by Quantrill and Hollaway (1998)

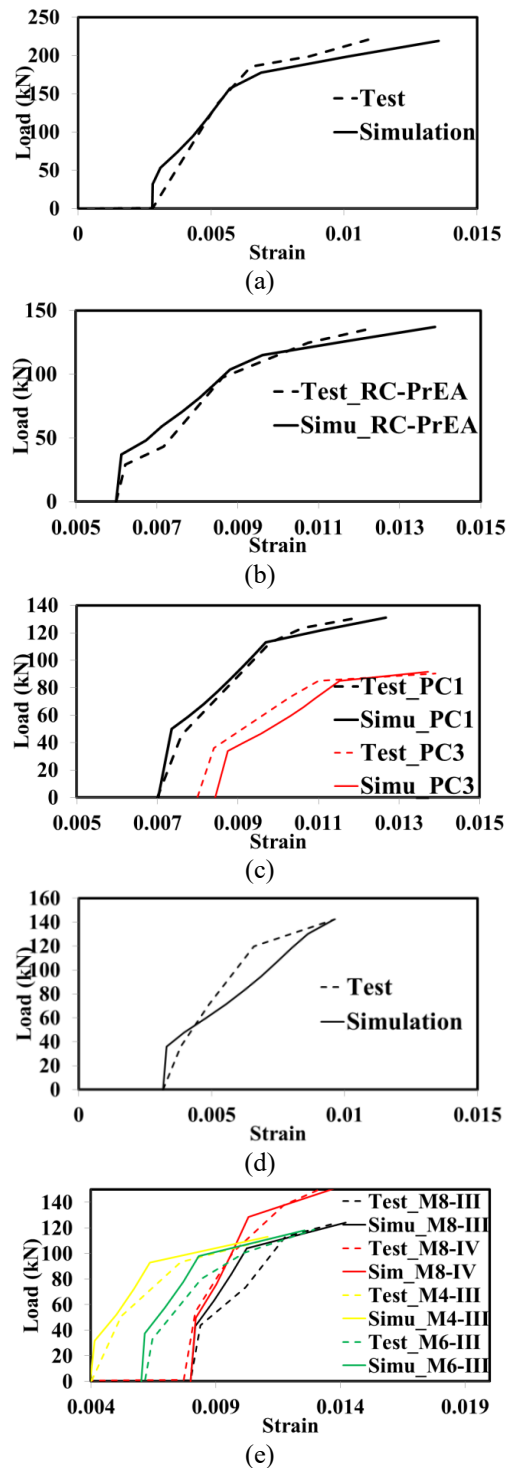


Fig. 6 FRP strain-Load curve for beam tested by (a) Yu *et al.* (2008) (b) Pelligrino *et al.* (2009) (c) PC-1 and PC-3 by Xue *et al.* (2010) (d) P4 tested by Quantrill and Hollaway (1998) (e) Woo *et al.* (2008)

area under the M/EI diagram between the corresponding points. The graphical representation of the theorem as shown in Fig. 3 can be expressed mathematically as follows

$$t_{A/B} = \bar{x} \int_A^B \frac{M}{EI} dx, \quad (17)$$

Table 1 Details of EBR strengthened Prestressed Beam

E	Specimen	P_f (kN)	Pre. %	Mat. type	l_{span} , mm	l_{shear} , mm	b, mm	h, mm	d, mm
Pelligrino and Modena (2009)	RC-PrEA	137.3	30	CFRP Laminate	9000	3200	300	500	425
Xue <i>et al.</i> (2010)	PC-1	131.1	42	CFRP plate	2500	950	150	250	210
	PC-3	91.6	50						
You <i>et al.</i> (2012)	PCFCB1-40	120	40	CFRP strips	2400	1200	200	300	249
	PCFCB1-60	119.6	60		6400	2300	400	600	549
	PFCB2-50	500	50						
Quantrill and Hollaway (1998)	P4	142.5	40	CFRP sheet	2200	845	130	230	180
Yu <i>et al.</i> (2008)	C	212	15	CFRP sheet	2130	710	203	305	265
Woo <i>et al.</i> (2008)	M4-III	112.7	40	CFRP plate	3000	1200	400	220	190
	M6-III	118.4	60						
	M8-III	125.1	80						
	M8-IV	151.9	80						

P_f : failure load ; Pre. %: prestressing percentage; l_{span} : total span; l_{shear} : shear span; b: beam width; h: Beam height; d: effective depth of beam

Table 2 Reinforcement Details of EBR strengthened Prestressed Beam

Author	Specimen	A_{st} , mm ²	A_{sc} , mm ²	f'_c , MPa	f_{y_s} , MPa	t_p , mm	A_p , mm ²	E_p , GPa
Pelligrino and Modena (2009)	RC-PrEA	708	307	71	375	1.2	96	166
Xue <i>et al.</i> (2010)	PC-1	420	56.5	52.3	350	1.2	70	150
	PC-3	339.2					28	
You <i>et al.</i> (2012)	PCFCB1-40	235.6	398	18	420	1.4	65	165
	PCFCB1-60							
	PFCB2-50	1906	850.5				140	
Quantrill and Hollaway (1998)	P4	314.15	100.5	45	556	1.3	117	135
Yu <i>et al.</i> (2008)	C	402.1	157.1	39	510	0.16	31.6	228
Woo <i>et al.</i> (2008)	M4-III							
	M6-III	603.2	157.1	26.4	400	1.4	70	165
	M8-III							
	M8-IV	850.6						

A_{st} : Area of ten. Steel; A_{sc} : Area of Compression steel ; f'_c : Compressive strength of concrete ; f_{y_s} : Yield strength of steel; t_p : thickness or diameter of FRP; A_p : Area of FRP; E_p : Elastic modulus of FRP

Where the denotations are clearly shown in Fig. 3. The whole procedure of M- κ analysis summarized as follows in Fig. 4.

2.3 Comparison of load-deflection and load versus FRP-strain for prestressed EBR strengthened beam

The validity of the proposed M- κ has been checked by the comparison of load-deflection and load-FRP strain curve reported in the literature. The load-deflection curve and FRP strain-load curve obtained using the methodology described above and illustrated in Fig. 4 is shown in Fig. 5 and Fig. 6 for EBR strengthened beam. The beam properties

Table 3 Details of NSM strengthened Prestressed Beam

Author	Specimen	P_f (kN)	Pre. %	Mat. type	l_{span} , mm	l_{shear} , mm	b, mm	h, mm	d, mm
Rezazadeh <i>et al.</i> (2014)	30% prestress	97.64	30	CFRP Laminate	2200	900	150	300	250
	40% prestress	87.80	40						
Nordin and Taljsten (2006)	BPS5	122	20	CFRP Rod	3600	1300	200	300	250
	BPM4	123	20						
Raafat and Mohamed (2011)	B2-20	141	20	CFRP	5000	2075	200	400	353
	B2-40	141.7	40						
	B2-60	134.7	60						
Peng <i>et al.</i> (2014)	PRS-EB	146.4	30	CFRP Plate CFRP Strip	3300	1200	150	350	314
	PRS-2N20	141.7	50						

P_f : failure load ; Pre. %: prestressing percentage; l_{span} : total span; l_{shear} : shear span; b: beam width; h: Beam height; d: effective depth of beam

Table 4 Reinforcement Details of NSM strengthened Prestressed Beam

Author	Specimen	A_{st} , mm ²	A_{sc} , mm ²	f'_c , MPa	f_{y_s} , MPa	t_p , mm	A_p , mm ²	E_p , GPa
Reza zadeh <i>et al.</i> (2014)	30% prestress	157.1	157.1	32.2	585	1.4	28	165
	40% prestress							
Nordin and Taljsten (2006)	BPS5	402.1	402.1	65	496	10	100	160
	BPM4							250
Raafat and Mohamed (2011)	B2-20							
	B2-40	603.2	157.1	40	475	9.5	70.9	124
	B2-60							
Peng <i>et al.</i> (2014)	PRS-EB	402.1	760.2	26.4	400	1.2	60	165
	PRS-2N20					2	64	131

A_{st} : Area of ten. Steel; A_{sc} : Area of Compression steel ; f'_c : Compressive strength of concrete ; f_{y_s} : Yield strength of steel; t_p : thickness or diameter of FRP; A_p : Area of FRP; E_p : Elastic modulus of FRP

are tabulated in Tables 1 and 2.

2.4 Comparison of load-deflection and load versus FRP-strain for NSM strengthened beam

This section shows the load-deflection and load-FRP strain comparison for beams prestressed with NSM reinforcement in Figs. 7 and 8. The beam properties are tabulated in Tables 3 and 4.

From the validation of load-deflection, load-FRP strain, it can be incurred that the present M- κ model can predict the load-deflection relationship with minor discrepancies which might be caused by the sensitive material properties, especially the tensile strength of concrete using empirical code relation from the quoted values of compressive strength. Based on this observation it can be concluded that the proposed M- κ model can predict the behaviour under loading with satisfactory precisions to be used as the basis for strain energy determination. The failure load obtained from this M- κ relation, for the beams that failed due to FRP rupture are compared in the later part of the paper showing

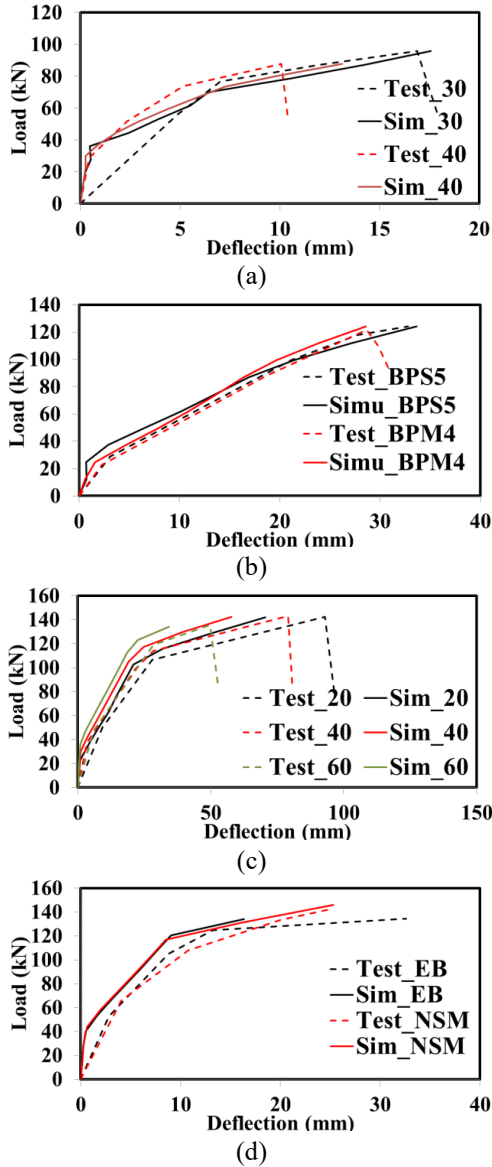


Fig. 7 Load versus deflection plot for beams tested by (a) Rezazadeh *et al.* (2014). (b) Nordin and Täljsten (2006) (c) Raafat and Mohamed (2011) (d) Peng *et al.* (2014)

good correlation and hence implies the good accuracy of the model.

3. Debonding failure analysis of prestressed beam

The existing experimental results show that applying prestressed CFRP for strengthening not only improves the load carrying capacity and cracking behaviour but also increases the debonding capacity of the plate. However, some beams still exhibit premature debonding failure. So, the focus of the current study is to predict the debonding load of beams.

3.1 Determining the ERR

Since it is already mentioned that the typical failure observed in prestressed beams are the IC type failure, so

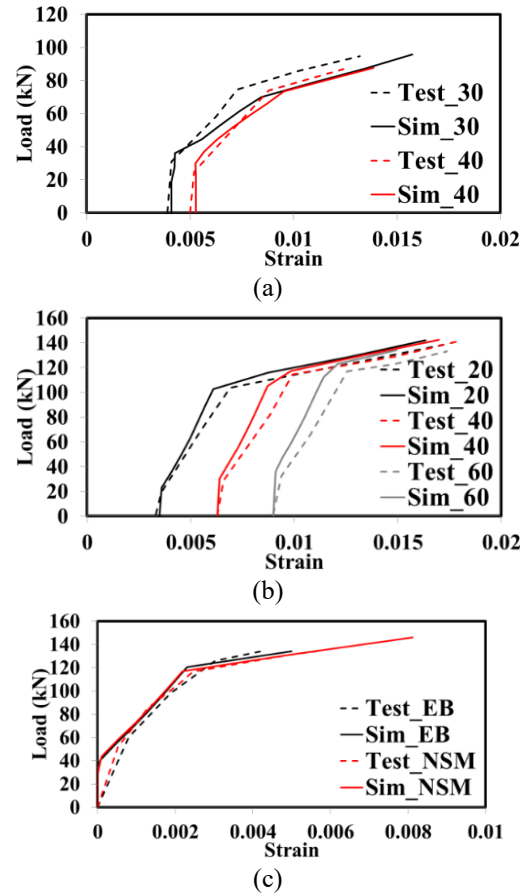


Fig. 8 FRP strain versus load plot for beams tested by (a) Rezazadeh *et al.* (2014). (b) Raafat and Mohamed (2011) (c) Peng *et al.* (2014)

this study will focus on the IC debonding analysis. Determination of ERR for IC debonding assumes that the FRP debonded from the beam soffit for EBR strengthening and the groove detached from the concrete attached to it in the case of NSM technique, at the location near the load point. Experimental evidence showed this location to be (0 to $h/2$) from the load point towards the shear span (Garden and Hollaway 1998). This partial detachment changes the FRP force due to flexure in the FRP reinforcement. But since the prestressing force is an external force, so there is no change in the prestressing force due to detachment. The FRP force due to flexure is then determined using extension compatibility. Steps to determine the force in the partially debonded region are as follows:

- Assuming an interface crack of the length of ' l_d '.
- Then a constant force, F_{ass} is assumed along the entire partially debonded region of length ' l_d '.
- Determining the M_{appcen} Using Eq. (8) for this F_{ass}
- Determine the curvature of the section for M_{appcen}
- Hence the strain of concrete at the level of FRP is determined for the whole length ' l_d '.

Eqs. (18) to (20) are used in steps (a) to (e). Total deformation of concrete in the partially debonded region

$$\Delta d = \int_{debonded} \varepsilon_{c_frp} dx \quad (18)$$

Average strain in concrete will be then

$$\frac{\Delta d}{L_{debonded}} = \int_{debonded} \frac{\varepsilon_{c-fRP}}{L_{debonded}} dx \quad (19)$$

As a result, the average stress of FRP, f_p , due to external load will be

$$f_p = E_f \cdot \frac{\Delta d}{L_{debonded}} \quad (20)$$

ε_{c-fRP} is the strain at concrete at the level of FRP due to bending only; Δd is the total extension in debonded zone and $L_{debonded}$ is the length of debonded zone.

Once the force in the partially debonded region is determined, the strain, curvature, depth of neutral axis can be determined using the concept described in the previous section. After determining these values, ERR can be calculated using the following Eqs. (21) to (28)

$$\delta W_{sys} = \sum_{critical\ zone} \delta W_{section} \quad (21)$$

$$\delta W_{section} = \delta W_b + \delta W_a + \delta W_p \quad (22)$$

$$\delta W_b = \frac{1}{2} (M_{1appcen} + M_{2appcen}) (\kappa_2 - \kappa_1) \quad (23)$$

$$\delta W_b = \frac{1}{2} (F_{1p} + F_{2p}) (\varepsilon_{20} - \varepsilon_{10}) \quad (24)$$

$$\delta W_p = \frac{1}{2} (F_{1p} + F_{2p}) (\varepsilon_{2p} - \varepsilon_{1p}) \quad (25)$$

$$\frac{\partial W_{sys}}{\partial a} = \frac{\delta W_{section}}{\delta a} \quad (26)$$

δW_b and δW_a are the work done on RC beam alone due to bending and axial strain; δW_p is the Work done on the FRP plate; $M_{1appcen}/M_{2appcen}$ are the moments acting on RC section about centroid axis; κ_2/κ_1 are the curvature of the RC section; $\varepsilon_{20}/\varepsilon_{10}$ are the strain at the equivalent centroid; F_{1p}/F_{2p} are the axial force in the FRP; $\varepsilon_{2p}/\varepsilon_{1p}$ are the Strain at the FRP level. The subscript 1 refers to state '1' i.e., state before infinitesimal debonding crack and subscript 2 refers to state '2' i.e., state after the infinitesimal debonding crack. The debonding crack is increased by 1 mm as was proposed by Achintha and Burgoyne (2008).

It is assumed in the analysis that the ERR occurs in that debonded zone due to the change FRP force. It should be mentioned here that Achintha and Burgoyne (2008) assumed a zone namely transition zone of 30 times thickness of FRP plate on both sides of the debonded zone. According to their analysis transition zone is the zone where the energy changes occur. The present analysis discards that transition zone for IC debonding analysis and concentrated on the energy change only in the debonded zone, as shown in Fig. 9, because it is found that the energy change in the transition zone is small with respect to the energy change in the debonded zone. The analysis with this assumption also gives good agreement with the experimental results.

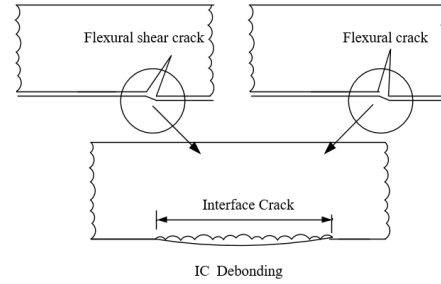


Fig. 9 Interface crack length for IC debonding modified from Achintha and Burgoyne (2008)

$$\frac{\partial W_{ext}}{\partial a} = \frac{\text{work done by external force (force * displacement)}}{\text{crack length}} = - \frac{P \delta \Delta}{\delta a} \quad (27)$$

$$G_R = \frac{1}{b_p} \left[\left| \frac{\partial W_{ext}}{\partial a} \right| - \left| \frac{\partial W_{sys}}{\partial a} \right| \right] \quad (28)$$

Where $\partial W_{ext}/\partial a$ is the rate of change of the work done by the external force and $W_{sys}/\partial a$ is the rate of change of stored elastic energy of the strengthened beam section, ∂a is the debonding crack length and b_p is the fracture surface, which is the width of the FRP for EBR strengthening and the whole width of beam for NSM strengthening details of which are described in another paper from paper author of author being processed (Hoque and Jumaat 2016).

3.2 Centroidal axis

As obvious from the previous section, determination of centroidal axis depth is required in order to determine the ERR. The moment about centroidal axis and strain at the centroidal axis is a necessary component for determination of ERR as obvious from the aforesaid section.

The centroidal axis at any stage will be

$$\alpha_{eff} = K_\alpha \alpha_{un} + (1 - K_\alpha) \alpha_{fc} \quad (29)$$

$$K_\alpha =$$

$$K_\alpha = (M_{cr-mid}/M_{applied-mid})^{3.5} \left[1 - \frac{\{M_{applied-mid} - M_{cr-mid}\}^{3.5}}{\{M_{yield-mid} - M_{applied-mid}\}} \right] \quad (30)$$

Where α_{un} and α_{fc} are the depth of centroidal axis for uncracked and yielded section respectively.

3.3 Failure criteria

Once the ERR is determined, next step is the determination of failure criteria. The nature of sudden IC debonding in beam indicates that the failure is triggered by an extremely short undetectable interface crack near the load application point as illustrated in Fig. 9. This can also be evidenced by the experimental results like Garden *et al.* (Garden and Hollaway 1998) where the author reported a vertical displacement of 2 mm just before failure. On the other hand, Quantrill and Hollaway (Quantrill and Hollaway 1998) reported a vertical displacement of 5 mm at the base of shear cracks which leads to failure. So, this

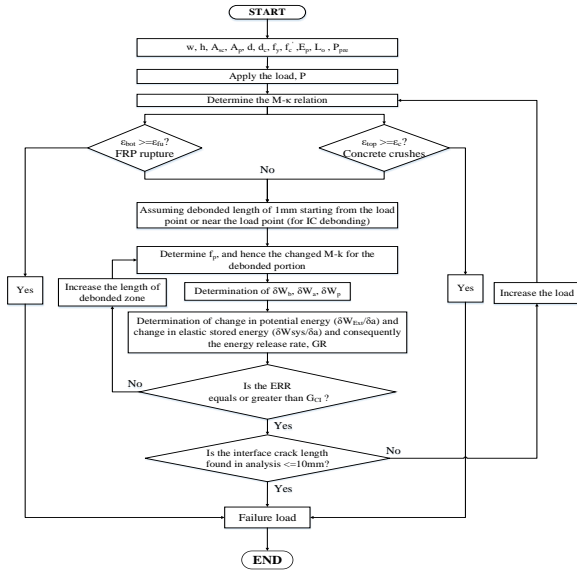


Fig. 10 Flowchart showing the determination of premature failure

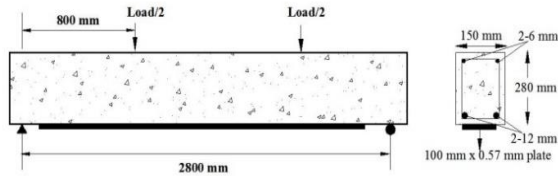


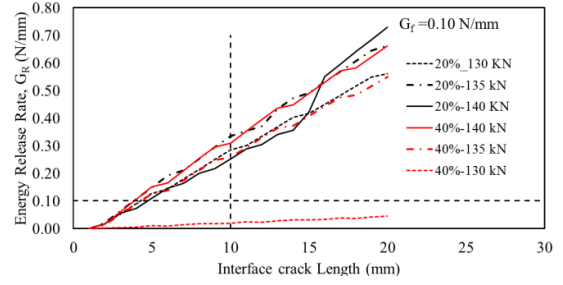
Fig. 11 Geometric details of assumed example beam

concept of short interface crack is considered in predicting the failure load in case of IC debonding. The analysis assumes that the load which can trigger debonding with very short interface crack length can cause failure. However, it is not trivial to suggest a specific critical crack length for complicated IC debonding type failure. However, the analysis is checked for different interface crack length such as 5, 10 mm etcetera and a critical interface crack length of 10 mm is thus chosen as the failure criterion as it estimates the failure load conservatively. It should also be mentioned here that Achintha and Burgoyne (2008) did not propose any specific failure criteria for predicting the debonding load.

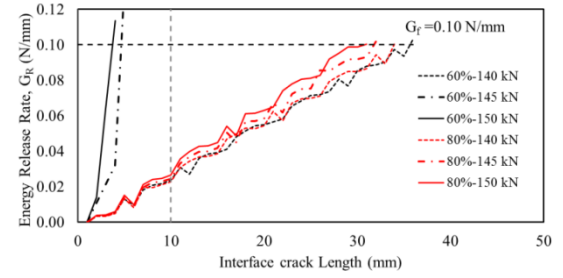
3.4 Fracture energy

Achintha and Burgoyne (2008) justified the use of mode I fracture energy as the governing failure both for PE failure and IC debonding failure. So, this paper also uses mode I fracture energy as the limiting criteria.

Though standard fracture test can provide the actual mode-I fracture energy of concrete, a reliable approximation can be done from simplified tension softening model and empirical models (Achintha and Burgoyne 2008). Among all the models, this analysis adopts the empirical relation provided by Bazant and Becq-Giraudon (2002) as in Eq. (31) to estimate the G_f value which is convenient to use and also correlates well with the tension softening models.



(a)



(b)

Fig. 12 Energy release rate versus interface crack length for IC debonding failure

$$G_f = 0.0025 \alpha_o \left(\frac{f'_c}{0.051} \right) \left(1 + \frac{d_a}{11.27} \right)^{0.22} \left(\frac{W}{C} \right)^{0.30} \left(\frac{N}{mm} \right) \quad (31)$$

Here α_o is a coefficient for aggregate type; f'_c is the concrete compressive strength; d_a is the aggregate size and w/c is the water cement ratio.

The entire procedure of determining the failure load is illustrated in Fig. 10.

3.5 Example

To illustrate the application of the model, an RC beams strengthened with a carbon fiber reinforced polymer (CFRP) plate and loaded as shown in Fig. 11 has been analyzed.

The compressive and tensile strength of concrete are taken as 35 MPa and 2.8 MPa respectively. The Young's modulus and steel stress of steel are taken as 200 MPa and 600 MPa respectively. The Young's modulus of CFRP is taken as 145 MPa and tensile strength of 2200 MPa. The unstrengthened capacity of the beam is 95 kN for steel yielding and after strengthening the capacity of the beam should be around 158 kN for FRP rupture. Since the premature failure of the prestressed beam occurs mostly in IC debonding mode, so the beam is analyzed with different prestressing level and checked how prestressing effect the IC debonding. Fig. 12 (a) shows the plotting of ERR versus interface crack length at different load near the ultimate strengthened capacity at the prestressing level of 20% and 40% and Fig. 12(b) shows that for the prestressing level of 60% and 80%. Plotting reveals that increase in the prestressing force increases the Interface crack length for a certain force. That implies an increase in failure load with the increase in prestressing force, according to the failure criteria.

3.6 Validation from experiment

This section shows the validation of experimental data which failed prematurely due to debonding. The properties of the beams are already mentioned earlier in Table 1 to Table 4. IC debonding analysis can be executed in MATLAB for different loads higher than yield capacity of the beam (termed as P_{simu} in this paper); hence the critical debonded zone length for that particular load can be determined, where ERR is equal to G_f . If the debonded zone length at the simulated load is less than or equal to 10 mm; failure is assumed to occur at that load otherwise the process will be continued by increasing load, till the theoretical failure load is obtained. The process is shown in Fig. 10 also. The following discussion is based on this methodology.

3.6.1 Yu *et al.* (2008)

Failure of prestressed beam C started by intermediate flexural cracks in the constant moment region and then a final failure occurred by the rupture of CFRP sheet at the end of CFRP sheets. IC debonding analysis was carried out to find the ERR and interface crack length at different load. Fig. 13 illustrates the interface crack length versus load ratio for beam C and the simulation result shows that the simulated load, P_{simu} is 90% of the experimental reported failure load, P_{Exp} according to analysis.

3.6.2 Pelligrino and Modena (2009)

Pelligrino and Modena tested a beam series to check the efficiency of strengthening with and without prestressed FRP laminate. The plotting in Fig. 14 shows the interface crack length versus load ratio, the plot for the beam simulated with prestressed FRP. The ratio of P_{simu}/P_{Exp} is 95% at the critical interface crack length of 10 mm.

3.6.3 Xue *et al.* (2010)

Two RC beams strengthened with prestressed CFRP plates, tested by Xue *et al.* are simulated here for debonding prediction and Fig. 15 shows the simulation results. For beam PC-1 sudden debonding of FRP sheet is reported. And analysis shows that the ratio of P_{simu}/P_{Exp} is 0.85, at the critical interface crack length of 10 mm. On the other hand, for beam PC-3 it can be seen from the plotting that predicted failure load is 97% of the reported experimental failure load.

3.6.4 You *et al.* (2012)

Beams with 40%, 60% prestressing tested by You *et al.* (2012) are simulated for debonding prediction. Interface crack length versus load ratio plot is shown in Fig. 16 for beam PFCB1-40 with 40% prestressing. The plotting shows that the predicted failure load is 73% of the reported debonding load. For beam PFCB1-60 the load ratio is 94% at the critical interface crack length of 10 mm. Whereas for beam PFCB2-50 as shown in Fig. 16 the load ratio is 98% at the critical interface crack length of 10 mm.

3.6.5 Peng *et al.* (2014)

Two beams tested by Peng *et al.* have been chosen for simulation. The beams have the same amount of strengthening reinforcement percentage but strengthened with different strengthening technique EBR and NSM. The

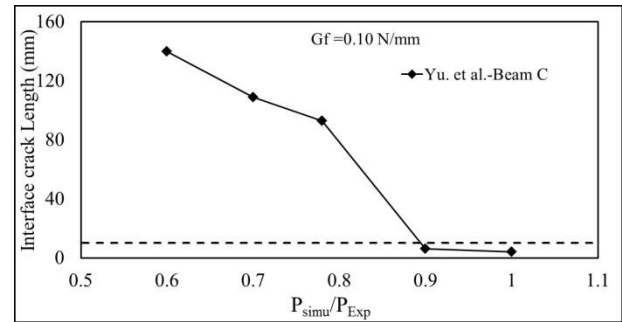


Fig. 13 Interface crack length versus Load ratio for Beam C

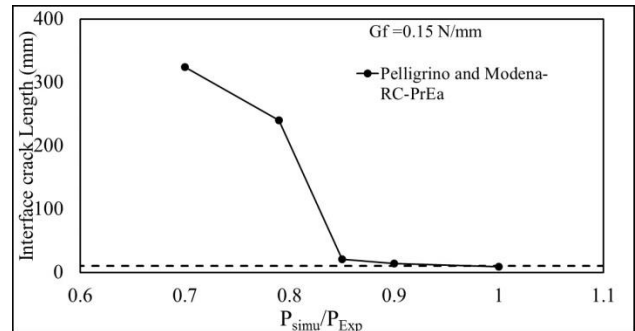


Fig. 14 Interface crack length versus Load ratio for Beams tested by Pelligrino and Modena (2009)

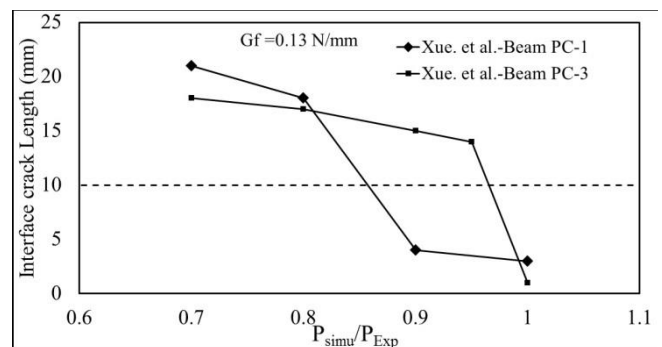


Fig. 15 Interface crack length versus Load ratio for beams tested by Xue *et al.* (2010)

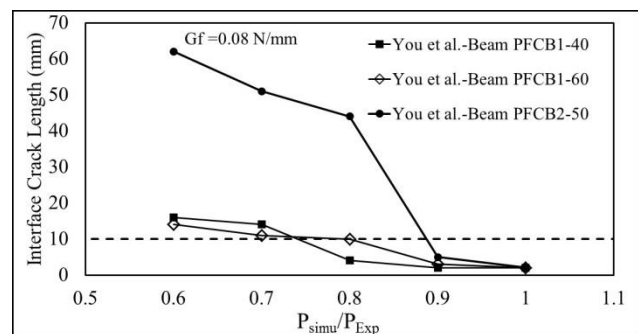


Fig. 16 Interface crack length versus Load ratio for beams tested by You *et al.* (2012)

failure of EBR strengthened beam initiated from the midspan of the beam. So, IC debonding analysis is checked for this beam as shown in Fig. 17.

It is clear from the Interface crack length versus load ratio plot that, the ratio of P_{simu}/P_{Exp} is 85% for EBR

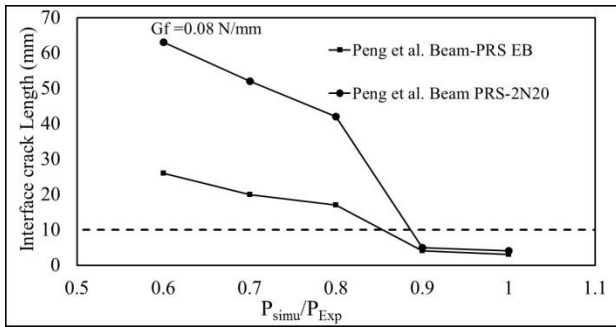


Fig. 17 Interface crack length versus Load ratio for beams tested by Peng *et al.* (2014)

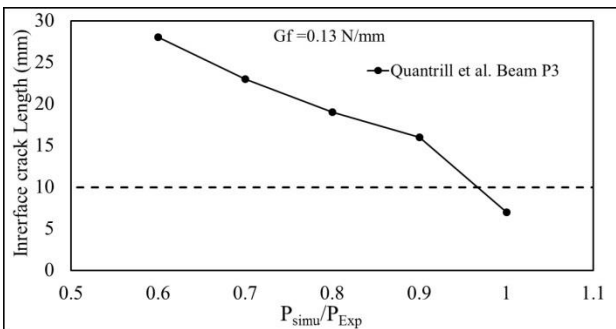


Fig. 18 Interface crack length versus Load ratio for beams tested by Quantrill and Hollaway (1998)

Table 5 Summary of experimental and simulated results

Beam ID	EFM	SFM	P _{theory}	P _{failure}	P _{theory} /P _{failure}
RC-PrEA	IC	IC	135	137.3	0.98
PC-1	IC	IC	112.5	131.1	0.86
PC-3	IC	IC	88.6	91.6	0.97
PCFCB1-40	IC	IC	88.7	120	0.74
PCFCB1-60	IC	IC	95	112.6	0.84
PB2-50	IC	IC	443	450	0.98
P4	IC	IC	138.3	142.5	0.97
C	IC	IC	189.5	212	0.89
PRS-EB	IC	IC	125.5	146.4	0.86
PRS-2N20	IC	IC	126	141.7	0.89
Rezazadeh <i>et al.</i> -30%	FR	FR	143.6	142	1.01
Rezazadeh <i>et al.</i> -40%	FR	FR	143.1	143	1.00
Hacha <i>et al.</i> 20%	FR	FR	143.3	135	1.06
Hacha <i>et al.</i> 40%	FR	FR	135	137.3	0.98

strengthened beam. For NSM strengthened beams the ratio of P_{simu}/P_{Exp} is 89%.

3.6.6 Quantrill and Hollaway (1998)

The prestressed beam P3 tested by Quantrill and Hollaway failed in the shear span. The plotting of interface crack length versus load ratio in Fig. 18 shows that the ratio of P_{simu}/P_{Exp} is 97%.

4. Results and discussions

Table 6 Effect of interface crack length on IC debonding failure prediction

Beam ID	P _{failure}	Interface Crack length 5 mm		Interface Crack length 7.5 mm		Interface Crack length 10 mm		Interface Crack length 15 mm	
		P _{Theory}	P _{Theory} /P _{failure}	P _{Theory}	P _{Theory} /P _{failure}	P _{Theory}	P _{Theory} /P _{failure}	P _{Theory}	P _{Theory} /P _{failure}
RC-PrEA	137.3	150	1.09	142	1.03	135	0.98	122.5	0.89
PC-1	131.1	117	0.89	115	0.88	112.5	0.86	107	0.82
PC-3	91.6	90	0.98	89	0.97	88.6	0.97	82	0.90
PCFCB1-40	120	95	0.79	100	0.83	88.7	0.74	78	0.65
PCFCB1-60	112.6	104	0.92	92	0.82	95	0.84	72	0.64
PB2-50	450	449	1.00	445	0.99	443	0.98	435	0.97
P4	142.5	145	1.02	142	1.00	138.3	0.97	129.5	0.91
C	212	198	0.93	190	0.90	189.5	0.89	188	0.89
PRS-EB	146.4	131	0.89	128	0.87	125.5	0.86	123.5	0.84
PRS-2N20	141.7	129	0.91	126.5	0.89	126	0.89	119	0.84

Hacha <i>et al.</i> 60%	FR	FR	117	113.2	1.03
Sang-M4-III	FR	FR	117	118.3	0.99
Sang-M6-III	FR	FR	117	155.6	0.75
Sang-M8-4	FR	FR	117	124.03	0.94
Sang-M8-3	FR	FR	81.63	94.8	0.86
Nordin-BPS5	FR	FR	81.63	87.8	0.93
Nordin-BPM4	FR	FR	113.8	124.2	0.92

EFM: Experimental failure mode; SFM: Simulated failure mode; FR: FRP rupture; IC: Intermediate crack induced debonding

Table 5 summarizes the simulated and experimental failure loads for beams strengthened using prestressed FRP that failed due to IC debonding obtained from literature as mentioned in Tables 1 to 4 by adopting both mode I fracture energy as the failure criteria. Fig. 19 shows the graphical comparison of experimental and simulated failure loads mentioned in Table 5. It is found that the mean of the ratio between simulated and experimental failure load is 0.93 with a standard deviation of 0.09.

Hence, from Table 5 and Fig. 19 it can be incurred that the model is efficient in predicting the failure load for beams strengthened using prestressed FRP that failed due to IC debonding with the assumption of 10 mm interface crack length. The model is also efficient in predicting the FRP rupture failure with different prestressing levels. The strain value, obtained for the theoretical debonding load using GEBA model, can be used as the limiting strain in real application of strengthened beams design, to prevent failure.

A comparison is also made to see the effect of limiting interface crack length on the failure load for beams failed in IC debonding, which is shown in Table 6. It can be seen from Table 6 that, if the limiting interface crack length is considered to be 5 mm the average failure load would be - 0.94 with a standard deviation of 0.08. On the other-hand if the limiting interface length is taken as 7.5 mm the average failure load is 0.92 with a standard deviation of 0.07. In case of interface crack length of 15 mm the average failure load is 0.83 with a standard deviation of 0.11. However,

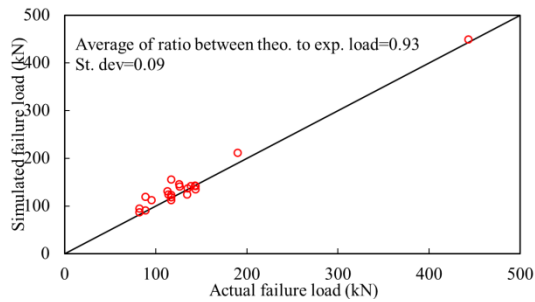


Fig. 19 Simulated versus experimental failure load

there is also chance of overestimation of failure load in case of interface crack length of 5, 7.5 and 15 mm. Based on these analyses it can be said that, the choice of 10 mm interface crack length is more safe and efficient for estimating debonding failure load.

5. Conclusions

GEBA analysis together with fracture mechanics criteria has been carried out to investigate the flexural as well as debonding behaviour of RC beams retrofitted with prestressed FRP.

The numerical approach considers the effect of external force applied to the beam due to prestressing. The necessary modification for computing ERR has also been taken properly in the analysis.

The accuracy of the prediction is checked with the published experimental results, taken from literature. For beams with prestressed FRP, the average of the ratio of theoretical to experimental load is 0.93 with a standard deviation of 0.09, by using GEBA model with a limiting interface crack length of 10mm. An analysis is also presented showing the sensitivity of results with different interface crack length and hence the choice of using 10 mm interface crack length is justified.

In practical application, the strain value obtained from the debonding analysis model can be used as a limiting strain value in designing to prevent IC debonding.

Finally, it can be incurred that GEBA analysis together with fracture energy criteria is highly prospective for premature debonding estimation of beams that need to be strengthened with prestressed FRP.

Acknowledgments

The authors are grateful for the financial support towards this research by The University of Malaya-Malaysia, High Impact Research Grant (HIRG) No. UM.C/625/1/HIR/MOHE/ENG/36 (16001-00-D000036)-“Strengthening Structural Elements for Load and Fatigue”.

References

Achintha, P. and Burgoyne, C. (2008), “Fracture mechanics of plate debonding”, *J. Compos. Constr.*, **12**(4), 396-404.

- Achintha, P. and Burgoyne, C.J. (2009), “Moment-curvature and strain energy of beams with external fiber-reinforced polymer reinforcement”, *ACI Struct. J.*, **106**(1), 20.
- ACI-4402R-08 (2008), *Guide for the Design and Construction of Externally Bonded FRP Systems for Strengthening Concrete Structures*, Farmington Hill, Michigan, U.S.A.
- ACI-CODE (2008), *Building Code Requirements for Structural Concrete*. Detroit, U.S.A.
- Barros, J.A., Taheri, M., Salehian, H. and Mendes, P.J. (2012), “A design model for fibre reinforced concrete beams pre-stressed with steel and FRP bars”, *Compos. Struct.*, **94**(8), 2494-2512.
- Bazant, Z.P. and Becq-Giraudon, E. (2002), “Statistical prediction of fracture parameters of concrete and implications for choice of testing standard”, *Cement Concrete Res.*, **32**(4), 529-556.
- Branson, D.E. (1968), *Design Procedures for Computing Deflections*, Am. Concrete Inst. Journal & Proceedings.
- Dai, J.G., Harries, K.A. and Yokota, H. (2008), “A critical steel yielding length model for predicting intermediate crack-induced debonding in FRP-strengthened RC members”, *Steel Compos. Struct.*, **8**(6), 457-473.
- El-Hacha, R., Wight, R. and Green, M. (2001), “Prestressed fibre-reinforced polymer laminates for strengthening structures”, *Progr. Struct. Eng. Mater.*, **3**(2), 111-121.
- Garden, H. and Hollaway, L. (1998), “An experimental study of the failure modes of reinforced concrete beams strengthened with prestressed carbon composite plates”, *Compos. Part B: Eng.*, **29**(4), 411-424.
- Ghasemi, S., Maghsoudi, A.A., Bengar, H.A. and Ronagh, H.R. (2015), “Flexural strengthening of continuous unbonded post-tensioned concrete beams with end-anchored CFRP laminates”, *Struct. Eng. Mech.*, **53**(6), 1083-1104.
- Gunes, O., Buyukozturk, O. and Karaca, E. (2009), “A fracture-based model for FRP debonding in strengthened beams”, *Eng. Fract. Mech.*, **76**(12), 1897-1909.
- Hajihashemi, A., Mostofinejad, D. and Azhari, M. (2011), “Investigation of RC beams strengthened with prestressed NSM CFRP laminates”, *J. Compos. Constr.*, **15**(6), 887-895.
- Hearing, B.P. (2000), “Delamination in reinforced concrete retrofitted with fiber reinforced plastics”, Ph.D. Dissertation, Massachusetts Institute of Technology, U.S.A.
- Hognestad, E. (1951), *Study of Combined Bending and Axial Load in Reinforced Concrete Members*, University of Illinois, Engineering Experiment Station, Bulletin, No. 399.
- Kara, I.F., Ashour, A.F. and Köroğlu, M.A. (2016), “Flexural performance of reinforced concrete beams strengthened with prestressed near-surface-mounted FRP reinforcements”, *Compos. Part B: Eng.*, **91**, 371-383.
- Lu, X., Teng, J., Ye, L. and Jiang, J. (2007), “Intermediate crack debonding in FRP-strengthened RC beams: FE analysis and strength model”, *J. Compos. Constr.*, **11**(2), 161-174.
- Malek, A.M., Saadatmanesh, H. and Ehsani, M.R. (1998), “Prediction of failure load of R/C beams strengthened with FRP plate due to stress concentration at the plate end”, *ACI Struct. J.*, **95**(2), 142-152.
- Matthys, S. (2000), *Structural Behaviour and Design of Concrete Members Strengthened with Externally Bonded FRP Reinforcement*, Ghent University, Belgium.
- Niu, H. and Wu, Z. (2001), “Interfacial debonding mechanism influenced by flexural cracks in FRP-strengthened beams”, *J. Struct. Eng.*, **47**, 1277-1288.
- Nordin, H. and Täljsten, B. (2006), “Concrete beams strengthened with prestressed near surface mounted CFRP”, *J. Compos. Constr.*, **10**(1), 60-68.
- Oehlers, D., Nguyen, N.T. and Bradford, M.A. (2000a), “Retrofitting by adhesive bonding steel plates to the sides of RC

- beams. Part 1: Debonding of plates due to flexure”, *Struct. Eng. Mech.*, **9**(5), 491-504.
- Oehlers, D., Nguyen, N.T. and Bradford, M.A. (2000b), “Retrofitting by adhesive bonding steel plates to the sides of RC beams. Part 2: Debonding of plates due to shear and design rules”, *Struct. Eng. Mech.*, **9**(5), 505-518.
- Oudah, F. and El-Hacha, R. (2011), “Fatigue strength prediction of RC beams strengthened in flexure using prestressed NSM CFRP strips”, *Spec. Publ.*, **275**, 1-20.
- Pellegrino, C. and Modena, C. (2009), “Flexural strengthening of real-scale RC and PRC beams with end-anchored pretensioned FRP laminates”, *ACI Struct. J.*, **106**(3), 319.
- Peng, H., Zhang, J., Cai, C. and Liu, Y. (2014), “An experimental study on reinforced concrete beams strengthened with prestressed near surface mounted CFRP strips”, *Eng. Struct.*, **79**, 222-233.
- Quantrill, R. and Holloway, L. (1998), “The flexural rehabilitation of reinforced concrete beams by the use of prestressed advanced composite plates”, *Compos. Sci. Technol.*, **58**(8), 1259-1275.
- Raafat, E.H. and Mohamed, G. (2011), “Flexural strengthening of reinforced concrete beams using prestressed, near-surface-mounted CFRP bars”, *PCI J.*, **56**(4), 134-151.
- Rahimi, H. and Hutchinson, A. (2001), “Concrete beams strengthened with externally bonded FRP plates”, *J. Compos. Constr.*, **5**(1), 44-56.
- Rezazadeh, M., Barros, J. and Costa, I. (2015), “Analytical approach for the flexural analysis of RC beams strengthened with prestressed CFRP”, *Compos. Part B: Eng.*, **73**, 16-34.
- Rezazadeh, M., Barros, J.A. and Ramezansafat, H. (2016), “End concrete cover separation in RC structures strengthened in flexure with NSM FRP: Analytical design approach”, *Eng. Struct.*, **128**, 415-427.
- Rezazadeh, M., Costa, I. and Barros, J. (2014), “Influence of prestress level on NSM CFRP laminates for the flexural strengthening of RC beams”, *Compos. Struct.*, **116**, 489-500.
- Rosenboom, O. and Rizkalla, S. (2008), “Modeling of IC debonding of FRP-strengthened concrete flexural members”, *J. Compos. Constr.*, **12**(2), 168-179.
- Sebastian, W.M. (2001), “Significance of midspan debonding failure in FRP-plated concrete beams”, *J. Struct. Eng.*, **127**(7), 792-798.
- Teng, J., Lu, X., Ye, L. and Jiang, J. (2004), *Recent Research on Intermediate Crack Debonding in FRP-Strengthened RC Beams*.
- Teng, J., Smith, S.T., Yao, J. and Chen, J. (2003), “Intermediate crack-induced debonding in RC beams and slabs”, *Constr. Build. Mater.*, **17**(6), 447-462.
- Teng, J., Zhang, J. and Smith, S.T. (2002), “Interfacial stresses in reinforced concrete beams bonded with a soffit plate: A finite element study”, *Constr. Build. Mater.*, **16**(1), 1-14.
- TR-55 (2012), *The Concrete Society (UK): Technical Report No. 55-Design Guidance for Strengthening Concrete Structures Using Fibre Composite Materials*.
- Wang, C. and Ling, F. (1998), “Prediction model for the debonding failure of cracked RC beams with externally bonded FRP sheets”, *Proceedings of the 2nd International Conference on Composites in Infrastructure*.
- Woo, S.K., Nam, J.W., Kim, J.H.J., Han, S.H. and Byun, K.J. (2008), “Suggestion of flexural capacity evaluation and prediction of prestressed CFRP strengthened design”, *Eng. Struct.*, **30**(12), 3751-3763.
- Xue, W., Tan, Y. and Zeng, L. (2010), “Flexural response predictions of reinforced concrete beams strengthened with prestressed CFRP plates”, *Compos. Struct.*, **92**(3), 612-622.
- You, Y.C., Choi, K.S. and Kim, J. (2012), “An experimental investigation on flexural behavior of RC beams strengthened with prestressed CFRP strips using a durable anchorage system”, *Compos. Part B: Eng.*, **43**(8), 3026-3036.

CC